Picosecond multiple-pulse experiments involving spatial and frequency gratings

Duppen, Koos; Wiersma, Douwe A.

Published in:
Journal of the Optical Society of America B-Optical Physics

DOI:
10.1364/JOSAB.3.000614

Publication date:
1986

Picosecond multiple-pulse experiments involving spatial and frequency gratings: a unifying nonperturbational approach

Koos Duppen* and Douwe A. Wiersma

Picosecond Laser and Spectroscopy Laboratory, Department of Physical Chemistry, University of Groningen, Nijenborgh 16, 9747 AG Groningen, The Netherlands

Received September 23, 1985; accepted November 19, 1985

The concept of a grating in real and frequency space is examined in the context of a three-pulse optical excitation cycle applied to a pseudo two-level model system. The calculations are done analytically using the Liouville-operator formalism in matrix form. It is shown that a continuous transition occurs from a grating in real space to a grating in frequency space when the first two excitation pulses separate in time. During this transition, the role of the population-relaxation time constant (T_1) is taken over by the dephasing time constant (T_2) bringing out the irreversible nature of the loss of coherence in an excited state. The underlying space–time transformation when moving from a grating in real space to a grating in frequency space further clarifies the loss in symmetry of the scattering pattern induced by a probe pulse by attributing it to the law of causality. It is finally concluded that the generalized grating concept is a powerful means of analyzing or predicting the effects of multiple-pulse multicolor optical-coherence experiments.

INTRODUCTION

The growing awareness in the scientific community of the tremendous potential of multiple-pulse optical-coherence experiments[1] for the study of spectral and dynamic features of absorbing species in the gas and the condensed phase is evident from the fast-growing number of papers dealing with such experiments. An interesting aspect of these experiments is that the time ordering of the excitation pulses determines or selects the state or transition whose dynamics is being studied by the coherent pump–probe cycle.[2] We recently showed, e.g.,[3] that in three-pulse, two-color experiments one moves continuously from one form of four-wave mixing, known as coherent Stokes Raman scattering, to others known as the three-transition echo and stimulated echo, depending only on the delay between resonant pulses at the different excitation frequencies. In a theoretical description of these and related four-wave mixing effects, it turned out to be quite useful to introduce the concept of grating in frequency space, especially to understand effects such as the accumulated photon echo,[4] the spin-stored optical echo,[5] and the different forms of two-color stimulated photon echoes.[6]

Spatial gratings obviously have played a crucial role in optical spectroscopy from their use in monochromators as dispersing elements to transient gratings[7] in time-resolved spectroscopy. The questions arise of what the relation is between the two different types of grating, one in real (physical) space and the other in frequency space, and what the information content is of each type of grating. All previous theoretical treatments of scattering from a spatial grating have used perturbation theory to describe the effect. In contrast, scattering from gratings in frequency space, the photon-echo effect, has always been dealt with in a nonperturbative fashion.

In this paper we address the question of what the formal relation is between the spatial and the frequency gratings using a model level system with three levels, two being coupled by the excitation field and the third acting as a bottleneck in the relaxation path. This type of level scheme is quite often encountered in practical situations. The calculations of the observables are done *nonperturbatively* by using the Liouville-operator formalism in matrix form. We show that a continuous transition occurs from the spatial to the frequency grating when the first two excitation pulses separate in time. One formally interesting point is that the loss of symmetry in the scattering event when one moves from the spatial to the frequency grating is due to causality. The analysis further shows that the scattering from a spatial and a frequency grating is conceptually identical, with time (t) playing the role of space (r) when we move from the spatial to the frequency grating. The overall conclusion is that the concept of a grating in physical or frequency space is a powerful means of analyzing multiple-pulse optical-coherence experiments.

Before continuing, we wish to inform the reader that related work on echo formation in gaseous media was done by Mossberg *et al.*[8] We further note that Fayer[9] recently reviewed the field of scattering experiments involving spatial gratings and that Weiner *et al.*[10] and De Silvestri *et al.*[11] have also considered the problem of three-pulse scattering in condensed absorbers. Finally, we wish to remind the reader of the fact that many of the concepts used in the field of optical-coherence experiments are known in the field of pulsed nuclear magnetic resonance (NMR), initiated by Hahn.[12] As in the latter case the sample dimension exceeds by far the wavelength of the radiation used, the spatial aspect of the emitted radiation is not considered. In NMR-imaging techniques, the spatial information is recovered by selective excitation of the nuclear spins in a spatially inhomogeneous magnetic field.

THEORETICAL APPROACH

Preliminaries

Optical-coherence experiments, as is well known, can be quite successfully described semiclassically by calculating

0740-3224/86/040614-08$02.00

the induced polarization $P(t)$ in the sample as a result of applying a number of excitation pulses. The resulting polarization then acts as a source term in Maxwell's equation to produce an outgoing field with a well-defined spatial direction. This beam can easily be detected by taking advantage of its spatial characteristics. Using the Markov approximation,[13] the induced polarization can be calculated as follows:

$$P(t) = N\langle\mu\rangle = N\,\mathrm{Tr}[\rho(t)\mu], \tag{1}$$

where μ_{nm} is the transition dipole (i.e., electric-dipole operator) between states $|n\rangle$ and $|m\rangle$ and N is the number density of the quantum-mechanical systems. The evolution of the density matrix obeys the Liouville–Von Neumann equation, which, for our purposes, can be written as

$$i\hbar\frac{\partial\rho}{\partial t} = [H_0, \rho] + [H_I, \rho] + i\hbar\left(\frac{\partial\rho}{\partial t}\right)_{\text{random}}, \tag{2}$$

where H_0 is the Hamiltonian of the unperturbed system

$$H_0 = \sum_n E_n|n\rangle\langle n| \tag{3}$$

while H_I describes the coupling of the system with the electromagnetic field. Within the dipole approximation, this interaction Hamiltonian is

$$H_I = -\frac{1}{2}\sum_i\sum_{n,m}\mu_{n,m}\cdot E_{0,i}(r,t) \times \exp\{-i[\omega_i t - k_i\cdot r + \phi_i]\}|n\rangle\langle m|. \tag{4}$$

The random interactions are usually averaged and described by phenomenological-damping terms[14]:

$$\left(\frac{\partial\rho_{nn}}{\partial t}\right)_{\text{random}} = \sum_m w_{mn}\rho_{mm} - \sum_m w_{nm}\rho_{nn}, \tag{5}$$

$$\left(\frac{\partial\rho_{nm}}{\partial t}\right)_{\text{random}} = -\Gamma_{nm}\rho_{nm}. \tag{6}$$

From the quantization of the reservoir,[15] it readily follows that the transition probabilities w obey the principle of detailed balance $w_{mn} = w_{nm}\exp(-\hbar w_{nm}/kT)$. If $\hbar\omega_{nm} \gg kT$, there are no upward transitions in the material system and the downward transitions correspond to spontaneous emission of photons or phonons.

The diagonal elements, in principle, relax in a combined fashion, leading to $d-1$ longitudinal relaxation times Γ_{nn}^{-1} when there are d energy levels. Each off-diagonal element decays with a characteristic transverse relaxation time Γ_{nm}^{-1}, which often has both adiabatic and nonadiabatic contributions. The former are due to random modulations of the energy differences $\hbar\omega_{nm}$, whereas the latter are caused by the finite lifetimes related to the transition probabilities out of states $|n\rangle$ and $|m\rangle$.

Summation of statistical averages for systems with different equations of motion must be performed after Eq. (2) has been integrated. Effects of inhomogeneous broadening can always be taken into account by integrating the final result of Eqs. (1) and (2) over a distribution of the resonant frequencies of the system under study.

Grating Scattering

The Level Structure

The accuracy of a calculation concerning any given nonlinear optical effect depends on the complexity of the level structure and the interaction Hamiltonian being discussed. The theory of two-level systems perturbed by a single (quasi-)monochromatic field is now well developed.[16,17] In Fig. 1, a three-level system is shown together with the relaxation rates among the levels. In our case, levels $|1\rangle$ and $|3\rangle$ may be the electronic ground and the first excited state of a molecule (S_0 and S_1), whereas level $|2\rangle$ is a vibrationally excited state in the S_1 manifold. If we assume that only states $|1\rangle$ and $|2\rangle$ are coupled through the coherent radiation field, the description of this system is analogous to that of a two-level system. The formation of the two-pulse photon echo and the three-pulse stimulated photon echo has been calculated by Hesselink[18] within such a three-level scheme. Following his calculation, we will describe the full response of the system to three consecutive short pulses resonant with the $|2\rangle \leftarrow |1\rangle$ transition. The similarity of stimulated photon echoes and transient holographic-grating experiments[9] will be stressed. The concepts of a population grating in r space and in the frequency domain, which will be developed in this section, form the basis of the description of the two-color photon echo and vibrational-grating scattering experiments reported in Refs. 3 and 19.

The Evolution of the Density Matrix

The time development of the system perturbed by a field at frequency ω is given by Eqs. (2)–(6). We obtain for the individual matrix elements of the level structure of Fig. 1

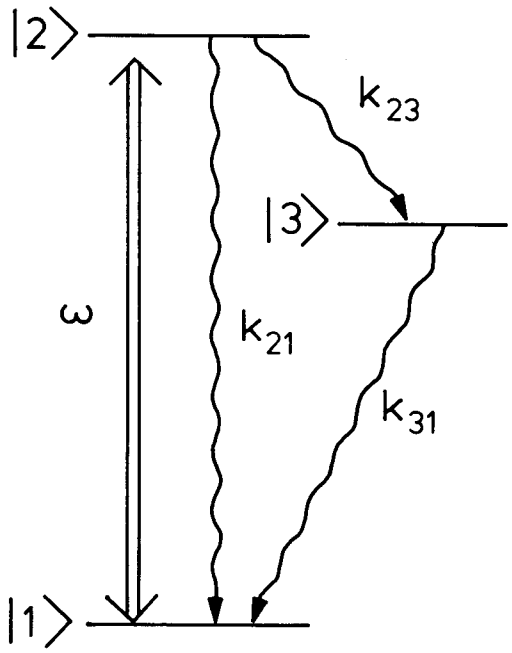

Fig. 1. Level scheme of a three-level system. Wavy arrows indicate decay channels. Level $|1\rangle$ and $|2\rangle$ are coupled by a radiation field at frequency ω.

$$\dot{\rho}_{11} = \frac{i\epsilon_{12}}{2}\{\tilde{\rho}_{21}\exp[-i(k\cdot r-\phi)] - \tilde{\rho}_{12}\exp[+i(k\cdot r-\phi)]\} + k_{21}\rho_{22} + k_{31}\rho_{33},$$

$$\dot{\tilde{\rho}}_{12} = \frac{i\epsilon_{12}}{2}(\rho_{22}-\rho_{11})\exp[-i(k\cdot r-\phi)] - \left(\frac{1}{T_2} - i\Delta\right)\tilde{\rho}_{12},$$

$$\dot{\tilde{\rho}}_{21} = \frac{i\epsilon_{12}}{2}(\rho_{11}-\rho_{22})\exp[+i(k\cdot r-\phi)] - \left(\frac{1}{T_2} + i\Delta\right)\tilde{\rho}_{21},$$

$$\dot{\rho}_{22} = \frac{i\epsilon_{12}}{2}\{\tilde{\rho}_{12}\exp[+i(k\cdot r-\phi)] - \tilde{\rho}_{21}\exp[-i(k\cdot r-\phi)]\} - (k_{21}+k_{23})\rho_{22},$$

$$\dot{\rho}_{33} = k_{23}\rho_{22} - k_{31}\rho_{33}. \tag{7}$$

Here ϵ_{12} is the Rabi frequency $\mu_{12}\cdot E_0(r,t)/\hbar$, and Δ is the detuning $\omega_{21}-\omega$. Going from Eqs. (2) to (7), a transformation was made to the rotating frame

$$\tilde{\rho}_{12} = \rho_{12}e^{-i\omega t}, \qquad \tilde{\rho}_{21} = \rho_{21}e^{+i\omega t}. \tag{8}$$

Then, after this transformation, all terms oscillating at the double frequency $\exp(+2i\omega t)$ were neglected. This is the so-called rotating-wave approximation (RWA). The transformation to the rotating frame is nothing but a change in representation from the Schrödinger picture to an interaction picture.[20] The RWA, however, neglects some physical phenomena, such as a small shift of the resonance frequency[17] and harmonic-generation effects.[21] However, when the optical frequency considerably exceeds the Rabi frequency and the detuning, the approximation is an extremely good one.[22] Equations (7) can be written compactly as

$$\dot{\rho} = iL\rho, \tag{9}$$

where ρ is a column vector with elements ρ_{11}, $\tilde{\rho}_{12}$, $\tilde{\rho}_{21}$, ρ_{22}, and ρ_{33} and L is a two-dimensional matrix called the Liouville operator.[23] The purpose of the transformation to the rotating frame and the RWA was to make L time independent. If we neglect the time dependence of the field envelope for the moment [see also Eq. (13)], the solution of Eq. (9) is simply

$$\rho(t) = e^{iLt}\rho(0). \tag{10}$$

The exponential operator can be calculated in matrix form by a method devised by Putzer[24]:

$$e^{iLt} = \sum_{j=0}^{n-1} r_{j+1}(t)P_j, \tag{11}$$

where $P_0 = 1$, $P_j = \Pi_{k=1}^{j}(iL - \lambda_k 1)$, and $\lambda_1 \ldots \lambda_n$ are the eigenvalues of iL in some arbitrary order. The functions $r(t)$ can be determined by solving the differential equations

$$\dot{r}_1 = \lambda_1 r_1, \qquad \dot{r}_j = r_{j-1} + \lambda_j r_j, \tag{12}$$

with $r_1(0) = 1$ and $r_j(0) = 0$.

In calculating the response of the system to three pulses, as shown in Fig. 2, there are two cases of interest. The exciting field is on: $e^{iLt} = A(\epsilon_{12}t)$, or the exciting field is off: $e^{iLt} = B(t)$. When very short excitation pulses are used, i.e., pulses with a coherent bandwidth larger than the (in)homogeneous linewidth of the transition studied, the assumptions of resonant excitation ($\Delta = 0$) and negligible decay during excitation can be made. With the field off, Δ describes the distribution of transition frequencies in the system.

Under these conditions, the temporal pulse shape is unimportant, and the effect of a pulse on the system can be completely described in terms of its area θ, where

$$\theta = \frac{\mu_{12}}{\hbar}\int E_0(r,t)\mathrm{d}t. \tag{13}$$

If we now apply Eqs. (11) and (12), we find for the two cases[25,26] that

$$A(\epsilon_{12}t) = A(\theta) = \frac{1}{2}\begin{bmatrix} 1+\cos\theta & -i\alpha^*\sin\theta & i\alpha\sin\theta & 1-\cos\theta & 0 \\ -i\alpha\sin\theta & 1+\cos\theta & (1-\cos\theta)\alpha^2 & i\alpha\sin\theta & 0 \\ i\alpha^*\sin\theta & (1-\cos\theta)(\alpha^*)^2 & 1+\cos\theta & -i\alpha^*\sin\theta & 0 \\ 1-\cos\theta & i\alpha\sin\theta & -i\alpha\sin\theta & 1+\cos\theta & 0 \\ 0 & 0 & 0 & 0 & 2 \end{bmatrix} \tag{14}$$

and

$$B(t) = \begin{bmatrix} 1 & 0 & 0 & 1-\beta\exp(-k_{31}t)+(\beta-1)\exp(-t/T_1) & 1-\exp(-k_{31}t) \\ 0 & \exp\left[\left(i\Delta-\frac{1}{T_2}\right)t\right] & 0 & 0 & 0 \\ 0 & 0 & \exp\left[\left(-i\Delta-\frac{1}{T_2}\right)t\right] & 0 & 0 \\ 0 & 0 & 0 & \exp(-t/T_1) & 0 \\ 0 & 0 & 0 & \beta\exp(-k_{31}t)-\beta\exp(-t/T_1) & \exp(-k_{31}t) \end{bmatrix}, \tag{15}$$

where $\alpha = \exp[-i(k\cdot r-\phi)]$, $\beta = k_{23}/(k_{21}+k_{23}-k_{31})$, $(T_1)^{-1} = k_{21}+k_{23}$, and T_2 contains an adiabatic part $(T_2)^{-1} = (T_2^*)^{-1} + (2T_1)^{-1}$. The evolution of the system when three pulses are applied can now be straightforwardly calculated by multiplication of the appropriate matrices:

$$\rho(t) = B(t)A(\theta_3)B(t_{23})A(\theta_2)B(t_{12})A(\theta_1)\rho(0). \tag{16}$$

When all molecules are initially in the ground state, we can take all $\rho_{nm}(0) = 0$, except for $\rho_{11}(0) = 1$.

From Eq. (1), it follows that the coherent radiative properties of the system are determined by the off-diagonal matrix elements ρ_{12} and ρ_{21}. Since $\rho_{21} = \rho_{12}^*$, we find for a homogeneously broadened ensemble that

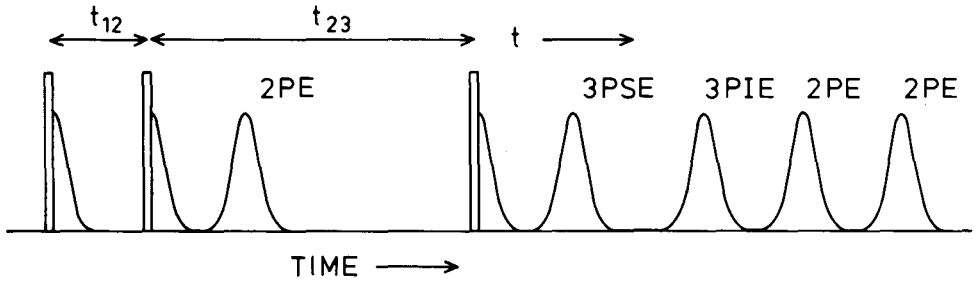

Fig. 2. Schematic diagram showing the various photon echoes and optical FID's produced by a sequence of three pulses. See Appendix A.

$$P(\Delta, t) = 2N\mu_{12}\,\mathrm{Re}[\rho_{12}(\Delta, t)]. \tag{17}$$

Using Eqs. (16) and (8), ρ_{12} can be evaluated at all times. The explicit expression for this matrix element when three pulses are applied is given in Appendix A. The terms that give rise to the various echoes and free-induction decays (FID's) of Fig 2 are indicated.

When there is a distribution of transition frequencies ω_{21}, the total polarization of the system is obtained by an integration over the inhomogeneous line

$$P(t) = \int_{-\infty}^{+\infty} g(\Delta)P(\Delta, t)\mathrm{d}\Delta. \tag{18}$$

Here $g(\Delta)$ is the inhomogeneous line-shape function. A Gaussian distribution is often observed, in which case we can write the normalized function

$$g(\Delta) = \frac{T_2'}{\sqrt{2\pi}}\exp(-\Delta^2 T_2'^2/2), \tag{19}$$

where T_2' is the inhomogeneous dephasing time.[27] When $T_2' \ll T_2$, the width of the distribution is $\Delta\omega = 2/T_2'\sqrt{2\ln 2}$ (FWHM).

Gratings in Frequency Space

In the remainder of this paper, we will be concerned only with the last term of the full expression for ρ_{12} listed in Appendix A:

$$\begin{aligned}\rho_{12}(\Delta, t) = -\frac{i}{8}\sin\theta_1 \sin\theta_2 \sin\theta_3[&(\beta - 2)\exp(-t_{23}/T_1) \\ &- \beta\exp(-k_{31}t_{23})]\exp[-(t_{12} + t)/T_2] \\ &\times (\exp[i\Delta(t - t_{12})]\exp\{+i[\omega t - (k_3 + k_2 - k_1)\cdot r \\ &+ (\phi_3 + \phi_2 - \phi_1)]\} \qquad (20a) \\ &+ \exp[i\Delta(t + t_{12})]\exp\{+i[\omega t - (k_3 + k_1 - k_2)\cdot r \\ &+ (\phi_3 + \phi_1 - \phi_2)]\}). \qquad (20b)\end{aligned}$$

This part of the off-diagonal element gives rise to a signal field that propagates in two different directions. As the time t_{23} is changed, information is obtained on the population-relaxation times of the system. Using Eqs. (18) and (19), the time dependence of the polarization at each delay t_{23} can be found for the two propagation directions:

(a) $k_s = k_3 + (k_2 - k_1)$:

$$P(t) \sim \exp[-(t_{12} + t)/T_2]\exp[-(t - t_{12})^2/2T_2'^2]. \tag{21}$$

The signal is at a maximum when $t = t_{12} - T_2'^2/T_2$, with the restriction that t must be positive. This is called the stimulated photon echo (3PSE). The time profile of the echo is the Fourier transform of the line shape for the transition at ω_{21}; the width of its amplitude is (FWHM)

$$\Delta t = 2T_2'\sqrt{2\ln 2}. \tag{22}$$

The FWHM of the echo intensity is $\Delta t/\sqrt{2}$.

(b) $k_s = k_3 + (k_1 - k_2)$:

$$P(t) \sim \exp[-(t_{12} + t)/T_2]\exp[-(t + t_{12})^2/2T_2'^2]. \tag{23}$$

This signal would have a maximum at $t = -t_{12} - T_2'^2/T_2$, if t could be negative. Taking a negative value of t, however, violates causality: The effect, which involves the third pulse, is present before the third pulse itself. This is the so-called virtual echo (3PVE). The magnitude of the signal immediately after the third pulse is as large as that of case (a). Whereas the polarization amplitude in case (a) increases to give the stimulated echo, when there is inhomogeneous broadening in the system the signal field in case (b) rapidly *decreases* with the inhomogeneous dephasing time T_2'. In the next section it will be shown that 3PSE and 3PVE merge when t_{12} approaches zero.

The dependence of both scattered signals on the time t_{23} is the same and can be found from Eqs. (20). For a pure two-level system (i.e., $\beta = 0$) the signal amplitude is proportional to

$$P(t) \sim \exp(-t_{23}/T_1). \tag{24}$$

For a system in which the upper state decays into a nondecaying level (i.e., $k_{21} = k_{31} = 0, \beta = 1$), the signal amplitude is proportional to

$$P(t) \sim 1 + \exp(-t_{23}/T_1). \tag{25}$$

The reason that population relaxation instead of dephasing determines the decay during time t_{23} is that the phase information that will give rise to the scattered signals of Eqs. (20) is contained in a modulation of the population in states $|1\rangle$ and $|2\rangle$ during that time. Two excitation pulses in succession on a particular transition generally produce a partially ordered population as a function of transition frequency, when there is inhomogeneous broadening present. This population modulation is also responsible for the Ramsay-fringe effect,[28] which is closely related to the 3PSE discussed here. The population difference $(\rho_{22} - \rho_{11})$ immediately after the second pulse $(t = t_{12}^+)$ is

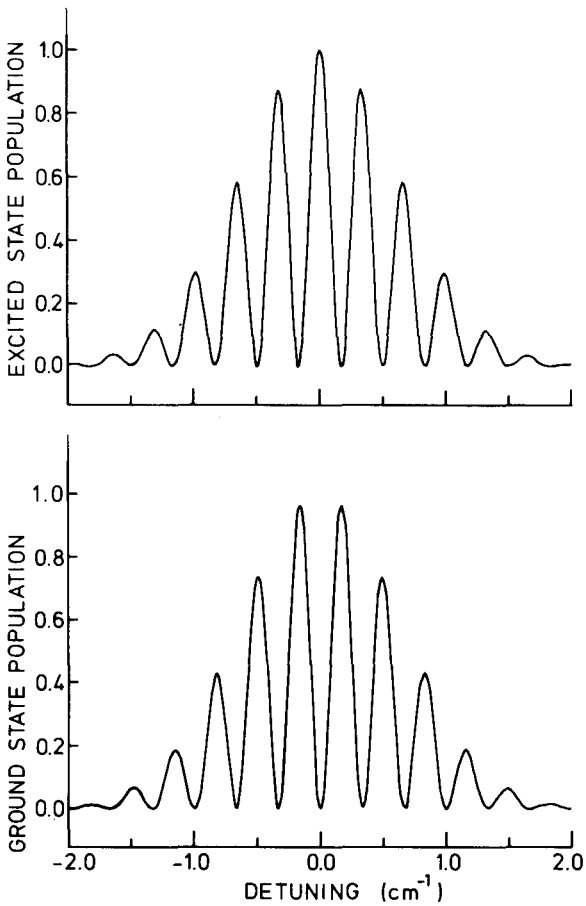

Fig. 3. Modulation of the population in states $|1\rangle$ and $|2\rangle$ after application of two resonant $\pi/2$ pulses separated by 100 psec. The horizontal axis gives the detuning from the line center. It does *not* indicate the absolute energy in either the ground or the excited state. The envelope of the modulation represents a line width of 1.5 cm^{-1}. The phase of the modulation was chosen to be zero.

$$
\begin{aligned}
(\rho_{22} - \rho_{11}) = \tfrac{1}{2}\{&\cos\theta_2[\beta\exp(-k_{31}t_{12}) \\
&- (\beta - 2)\exp(-t_{12}/T_1) - 2] + \cos\theta_1\cos\theta_2 \\
&\times [(\beta - 2)\exp(-t_{12}/T_1) - \beta\exp(-k_{31}t_{12})] \\
&+ 2\sin\theta_1\sin\theta_2\exp(-t_{12}/T_2) \\
&\times \cos(\Delta t_{12} - k_{12}\cdot r + \phi_{12})\}. \qquad (26)
\end{aligned}
$$

Here t_{12}, k_{12}, and ϕ_{12} are the time, **k**-vector, and phase differences between the two pulses.[29] The interaction of the third pulse with the frequency-domain population grating, described by the last part of Eq. (26), gives the off-diagonal element of Eqs. (20). The populations ρ_{11} and ρ_{22} are shown in Fig. 3 as a function of detuning for the case of maximum modulation ($\theta_1 = \theta_2 = \pi/2$ and $T_2 > t_{12}$). Longer pulse separation t_{12} produces more-rapid modulations of the population as a function of Δ. The phase of this grating in frequency space is a function of the position in r space. Population relaxation and spectral diffusion will tend to erase the grating, so that the detected signals get weaker when the delay t_{23} of the third pulse is increased.

Spatial Gratings

As the pulse separation t_{12} approaches zero, the character of the scattering process changes considerably. The grating in frequency space disappears completely, and instead a population grating in real space is formed. Two time-coincident interfering light beams produce a spatial interference pattern reproducing the intensity pattern of the intersecting excitation beams. In Fig. 4 such a spatial modulation is shown schematically.

This interference pattern will cause a spatially modulated population distribution through which the delayed third pulse experiences a spatially modulated transmission. The resulting Bragg scattering is sometimes called transient holographic-grating scattering since the spatially modulated structure in the sample (the hologram, optical absorption grating, or amplitude grating) was induced by two interfering light beams. In Fig. 4 the wave vector of the grating is along the y axis, and the associated wavelength is

$$\Lambda_{\text{grating}} = \frac{\lambda_{\text{light}}}{2\sin\theta}. \qquad (27)$$

The population grating is still described by Eq. (26) now with $t_{12} = 0$. Under these circumstances, the difference in time behavior of the signals, previously called 3PSE and 3PVE, disappears. Both signal fields are coincident with the third pulse and decay, according to Eqs. (18)–(20), as

$$P(t) \sim \exp(-t/T_2)\exp(-t^2/2T_2'^2). \qquad (28)$$

The dependence of the signals on the delay time t_{23} is the same as before. In Fig. 5, a grating scattering experiment on an inhomogeneously broadened transition is shown. For illustrative purposes, a phase-matching configuration was chosen in which the third beam is in the middle of the two beams that induce the grating. A finite wave-vector mismatch, equal for the two scattering directions, is the result of this geometry.

The following picture for the scattering process now emerges: When $t_{12} = 0$, a volume population grating is set up by the two excitation pulses. Part of the third pulse scatters symmetrically to both sides because of the spatially modulated transmission. As the second pulse is delayed with respect to the first pulse, inhomogeneous dephasing

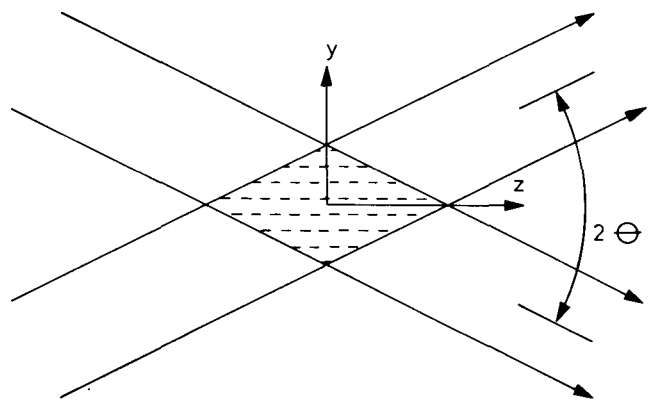

Fig. 4. Schematic representation of the interference pattern of two crossed monochromatic beams. A third beam can scatter from the resulting transient hologram.

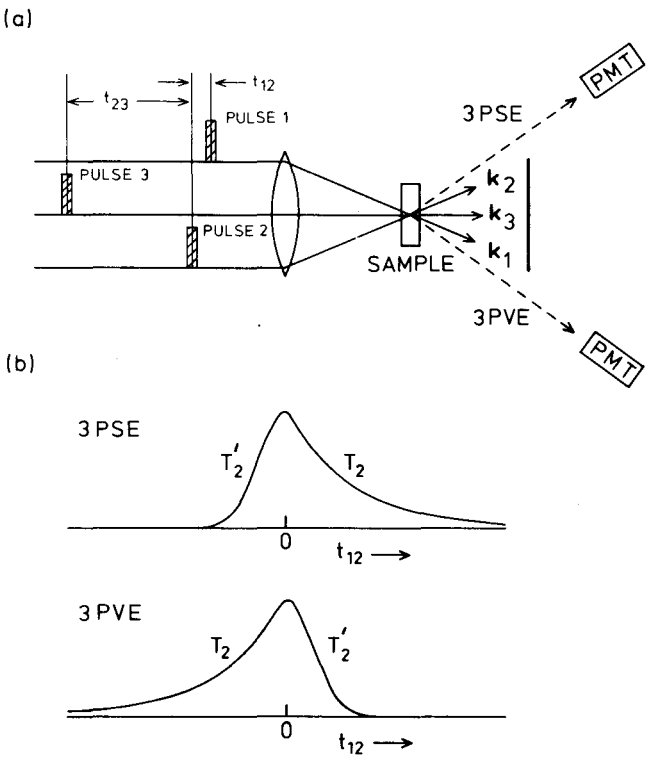

Fig. 5. (a) Grating scattering experiment. The two scattering directions are denoted by 3PSE and 3PVE. The observed intensity of the two signals is equal when $t_{12} = 0$. PMT, photomultiplier tube. (b) Scattering intensity as a function of the delay t_{12} for an inhomogeneously broadened transition ($T_2 > T_2'$). The delay t_{23} is assumed to be large ($t_{23} \gg t_{12}$). The decay on one side is determined predominantly by T_2 and on the other side by T_2'.

will occur in the time t_{12} between the pulses, and hence the spatial grating will be erased and replaced by a frequency grating. It is thus reasonable to speak of a spatial grating when $t_{12} < T_2'$ and of a frequency grating when $t_{12} > T_2'$. Of course, the change is gradual and is fully described by Eq. (26).

When t_{12} is so large that no spatial modulation is left at all, the third pulse will not induce a diffracted signal instantaneously. It will set rephasing in action, however, which nullifies the effect of inhomogeneous broadening during t_{12}. At the time $t = t_{12} - T_2'^2/T_2$, the spatial structure is recovered, and a macroscopic polarization results. From this point of view, the signal can be looked on as a case of delayed transient holographic-grating scattering. Because of the time ordering of the pulses that induce the grating, the spatial symmetry is lost, and scattering is possible in only one direction: the 3PSE. Scattering in the other direction has become virtual. As the excitation pulses are scanned in time through one another with the delay t_{23} large, signal intensities of the form of Fig. 5(b) result.

Both kinds of grating scattering experiment are often employed in studying the population dynamics of a particular system by varying the time t_{23}. We end this section by briefly reviewing the use that can be made of studying the decay of the spatial and the frequency grating.

Spatial-Grating Scattering (1) Gives a signal only spatially separated from the exciting beams; therefore good optical quality samples and strong signals are mandatory. (2) Can be used to study population relaxation and spatial diffusion of excitation. (3) Can be used in cases in which dephasing times are quite short and inhomogeneous broadening is negligible.

Frequency-Grating Scattering (3PSE's) (1) Gives a signal spatially and temporarily separated from the exciting beams; optical gating is possible. (2) Can be used to study population relaxation, spectral diffusion of excitation, and phase relaxation. (3) Can be used only on systems with finite dephasing times ($T_2 > t_{12}$) and sufficient inhomogeneous broadening ($T_2' < t_{12}$).

CONCLUSIONS

The nonperturbative treatment of three-pulse optical experiments shows that spatial- and frequency-grating scattering experiments are intimately related to each other through a space–time transformation. It is shown that the transition from a spatial to a frequency grating is continuous, as the first two excitation pulses are separating in time. In this transition, the role of the population-relaxation time (T_1) is taken over by the optical-dephasing time (T_2). At the same time, the symmetry of the scattering pattern gets lost. These features emphasize the irreversible nature of events that occur and the fact that physical laws are governed by causality. Finally, this analysis shows that the grating concept is universal and that it is a powerful tool in analyzing or predicting the effect(s) of multiple-pulse optical-coherence experiments. There is a long way to go, but optical-coherence pulse experiments are on the road to exploring the full information content of optical spectra.

APPENDIX A: OFF-DIAGONAL MATRIX ELEMENT ρ_{12}

Matrix element ρ_{12} pertinent to the pulse sequence of Fig. 2 applied to the level structure shown in Fig. 1:

FID, pulse 1:

$$\rho_{12}(t_{12} + t_{23} + t) = -\frac{i}{8}\sin\theta_1(\cos\theta_2 + 1)(\cos\theta_3 + 1) \times \exp[-(t_{12} + t_{23} + t)/T_2] \times \exp[+i\Delta(t_{12} + t_{23} + t)] \times \exp[+i(\omega t - k_1 \cdot r + \phi_1)],$$

FID, pulse 2:

$$-\frac{i}{8}\sin\theta_2(\cos\theta_3 + 1)\{2 + (\cos\theta_1 - 1) \times [\beta\exp(-k_{31}t_{12}) - (\beta - 2) \times \exp(-t_{12}/T_1)]\} \times \exp[-(t_{23} + t)/T_2]\exp[+i\Delta(t_{23} + t)] \times \exp[+i(\omega t - k_2 \cdot r + \phi_2)],$$

FID, pulse 3:

$$
\begin{aligned}
&-\frac{i}{8}\sin\theta_3(4+(\cos\theta_1-1)\\
&\times\{2\beta\exp[-k_{31}(t_{12}+t_{23})]-\cos\theta_2\\
&\times(2\beta-4)\exp[-(t_{12}+t_{23})/T_1]\}\\
&+(\cos\theta_2-1)[2\beta\exp(-k_{31}t_{23})\\
&-(2\beta-4)\exp(-t_{23}/T_1)]\\
&+(\cos\theta_1-1)(\cos\theta_2-1)\\
&\times\{\beta^2\exp[-k_{31}(t_{12}+t_{23})]\\
&+(\beta^2-2\beta)\exp[-(t_{12}+t_{23})/T_1]\\
&-(\beta^2-2\beta)\exp(-t_{12}/T_1)\exp(-k_{31}t_{23})\\
&-(\beta^2-2\beta)\exp(-k_{31}t_{12})\exp(-t_{23}/T_1)\})\\
&\times\exp(-t/T_2)\exp(+i\Delta t)\\
&\times\exp[+i(\omega t-k_3\cdot r+\phi_3)],
\end{aligned}
$$

Photon echo (2PE), pulses 1 and 2:

$$
\begin{aligned}
&-\frac{i}{8}\sin\theta_1(\cos\theta_2-1)(\cos\theta_3+1)\\
&\times\exp[-(t_{12}+t_{23}+t)/T_2]\\
&\times\exp[+i\Delta(t_{23}+t-t_{12})]\\
&\times\exp\{+i[\omega t-(2k_2-k_1)\cdot r\\
&+(2\phi_2-\phi_1)]\},
\end{aligned}
$$

2PE, pulses 1 and 3:

$$
\begin{aligned}
&-\frac{i}{8}\sin\theta_1(\cos\theta_2+1)(\cos\theta_3-1)\\
&\times\exp[-(t_{12}+t_{23}+t)/T_2]\\
&\times\exp[+i\Delta(t-t_{12}-t_{23})]\\
&\times\exp\{+i[\omega t-(2k_3-k_1)\cdot r\\
&+(2\phi_3-\phi_1)]\},
\end{aligned}
$$

2PE, pulses 2 and 3:

$$
\begin{aligned}
&-\frac{i}{8}\sin\theta_2(\cos\theta_3-1)\{2-(1-\cos\theta_1)\\
&\times[\beta\exp(-k_{31}t_{12})\\
&-(\beta-2)\exp(-t_{12}/T_1)]\}\\
&\times\exp[-(t_{23}+t)/T_2]\exp[+i\Delta(t-t_{23})]\\
&\times\exp\{+i[\omega t-(2k_3-k_2)\cdot r\\
&+(2\phi_3-\phi_2)]\},
\end{aligned}
$$

Image echo (3PIE) start of Carr–Purcell echo train, all pulses:

$$
\begin{aligned}
&-\frac{i}{8}\sin\theta_1(\cos\theta_2-1)(\cos\theta_3-1)\\
&\times\exp[-(t_{12}+t_{23}+t)/T_2]\\
&\times\exp[+i\Delta(t-t_{23}+t_{12})]\\
&\times\exp\{+i[\omega t-(2k_3-2k_2+k_1)\cdot r\\
&+(2\phi_3-2\phi_2+\phi_1)]\},
\end{aligned}
$$

Stimulated echo (3PSE) and virtual echo (3PVE), all pulses:

$$
\begin{aligned}
&-\frac{i}{8}\sin\theta_1\sin\theta_2\sin\theta_3[(\beta-2)\\
&\times\exp(-t_{23}/T_1)-\beta\exp(-k_{31}t_{23})]\\
&\times\exp[-(t_{12}+t)/T_2]\\
&\times(\exp[i\Delta(t-t_{12})]\exp\{+i[\omega t-(k_3\\
&-k_1+k_2)\cdot r+(\phi_3-\phi_1+\phi_2)]\}\\
&+\exp[i\Delta(t+t_{12})]\exp\{+i[\omega t-(k_3\\
&-k_2+k_1)\cdot r+(\phi_3-\phi_2+\phi_1)]\});
\end{aligned}
$$

$$\beta=\frac{k_{23}}{k_{21}+k_{23}-k_{31}},$$

$$(T_1)^{-1}=k_{21}+k_{23},$$

$$(T_2)^{-1}=(2T_1)^{-1}+(T_2{}^*)^{-1}.$$

ACKNOWLEDGMENTS

This research was supported by the Foundation of Chemical Research with financial aid from the Netherlands Organization for the Advancement of Pure Research. We gratefully acknowledge critical perusal of the manuscript by H. B. Levinsky.

* Present address, Koninklijke Shell Laboratorium Amsterdam, Badhuisweg 3, 1031 CM Amsterdam, The Netherlands.

REFERENCES AND NOTES

1. I. D. Abella, N. A. Kurnit, and S. R. Hartmann, Phys. Rev. Lett. **13,** 567 (1964); Phys. Rev. **41,** 391 (1966).
2. P. Ye and Y. R. Shen, Phys. Rev. A **25,** 2183 (1982).
3. K. Duppen, D. P. Weitekamp, and D. A. Wiersma, Chem. Phys. Lett. **106,** 147 (1984); **108,** 551 (1984).
4. W. H. Hesselink and D. A. Wiersma, Phys. Rev. Lett. **43,** 1991 (1979); J. Chem. Phys. **75,** 4192 (1981).
5. J. B. W. Morsink, W. H. Hesselink, and D. A. Wiersma, Chem. Phys. Lett. **64,** 1 (1979).
6. D. A. Wiersma, D. P. Weitekamp, and K. Duppen, in *Ultrafast Phenomena IV*, D. H. Auston and K. B. Eisenthal, eds. (Springer-Verlag, Berlin, 1984), p. 224.
7. H. Eichler and H. Stahl, J. Appl. Phys. **44,** 3429 (1973), and references therein.
8. T. W. Mossberg, R. Kachru, S. R. Hartmann, and A. M. Flusberg, Phys. Rev. A **20,** 1976 (1979).
9. M. D. Fayer, Ann. Rev. Phys. Chem. **33,** 63 (1982).

10. A. M. Weiner, S. De Silvestri, and E. P. Ippen, J. Opt. Soc. Am. B **2,** 654 1985).
11. S. De Silvestri, A. M. Weiner, J. G. Fujimoto, and E. P. Ippen, Chem. Phys. Lett. **112,** 195 (1984).
12. E. L. Hahn, Phys. Rev. **80,** 580 (1950).
13. For a recent discussion of this approximation, see Ph. de Bree, Ph.D. dissertation (University of Groningen, Groningen, The Netherlands, 1981).
14. N. Bloembergen and Y. R. Shen, Phys. Rev. **133,** A37 (1964).
15. N. Bloembergen, *Nonlinear Optics* (Benjamin, New York, 1965), Chap. 2.
16. R. L. Schoemaker, in *Laser and Coherence Spectroscopy*, J. I. Steinfeld, ed. (Plenum, New York, 1978).
17. L. Allen and J. H. Eberly, *Optical Resonance and Two-Level Atoms* (Wiley, New York, 1975).
18. W. H. Hesselink, Ph.D. dissertation (University of Groningen, Groningen, The Netherlands, 1980).
19. D. P. Weitekamp, K. Duppen, and D. A. Wiersma, Chem. Phys. Lett. **102,** 139 (1983).
20. Not *the* interaction picture. The connection between this rotating frame picture and the conventional interaction picture is $\tilde{\rho}_{12} = \exp[+i(\omega_{21} - \omega)t]\rho_{12}^{\mathrm{INT}}$ and $\tilde{\rho}_{21} = \exp[-i(\omega_{21} - \omega)t]\rho_{21}^{\mathrm{INT}}$.
21. E. Arimondo and G. Moruzzi, J. Phys. B **6,** 2382 (1973).
22. See, for instance, R. Loudon, *The Quantum Theory of Light* (Clarendon, Oxford, 1983), Chap. 2.
23. U. Fano, Phys. Rev. **131,** 259 (1963).
24. E. J. Putzer, Am. Math. Monthly **73,** 2 (1966).
25. W. H. Hesselink and D. A. Wiersma, J. Chem. Phys. **73,** 648 (1980).
26. W. H. Hesselink and D. A. Wiersma, J. Chem. Phys. **75,** 4192 (1981).
27. In this definition, the decay of the amplitude of an optical FID is $P_{\mathrm{FID}}(t) \sim \exp(-t^2/T_2)\exp(-t/2T_2')$.
28. M. M. Salour and C. Cohen-Tannoudji, Phys. Rev. Lett. **38,** 757 (1977).
29. In some published papers $\rho_{11}(t_{12}^{+})$ was written for a situation in which population relaxation is negligible on the time scale of the pulse separation t_{12}. This limitation was not always pointed out, however [e.g., K. Duppen, D. P. Weitzkamp, and D. A. Wiersma, Chem. Phys. Lett. **108,** 551 (1984); K. Duppen, L. W. Molenkamp, and D. A. Wiersma, Physica **127B,** 349 (1984)]. The correct, general, expression for ρ_{11} is

$$\rho_{11}(t_{12}^{+}) = \tfrac{1}{4}\{2 - \beta\exp(-k_{31}t_{12} + \beta\exp(-t_{12}/T_1) + \cos\theta_1 \times [\beta\exp(-k_{31}t_{12}) - \beta\exp(-t_{12}/T_1] + \cos\theta_2 \times [2 - \beta\exp(-k_{31}t_{12}) + (\beta - 2)\exp(-t_{12}/T_1)] + \cos\theta_1\cos\theta_2[\beta\exp(-k_{31}t_{12}) - (\beta - 2) \times \exp(-t_{12}/T_1)] - 2\sin\theta_1\sin\theta_2 \times \exp(-t_{12}/T_2)\cos(\Delta t_{12} - k_{12}\cdot r + \phi_{12})]\}.$$

Koos Duppen

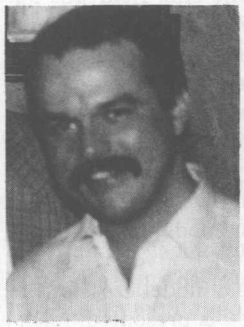

Koos Duppen was born in 1953 in Winterswijk, The Netherlands. He received both the *doctorandus* and Ph.D. degrees from the University of Groningen in 1980 and 1985, respectively. His thesis work with D. A. Wiersma was concerned with the vibrational dynamics in solids studied by time-resolved coherent Raman scattering effects and several type of photon echoes. Currently he is doing research in the Royal Dutch Shell Laboratories in Amsterdam.

Douwe A. Wiersma

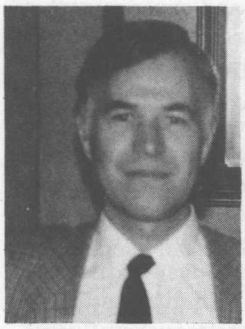

Douwe A. Wiersma, Professor of Physical Chemistry at the State University of Groningen, was born in 1943 in Amsterdam, The Netherlands. Since 1974 he has been involved with optical coherence effects, such as photochemical hole burning and photon echoes, in solids. His research interests lie both in the development of new optical coherence phenomena and in the application of these techniques to a variety of challenging spectroscopic problems. Most of his past work concerns the optical dynamics of molecular solids, while more recently dynamical studies of doped semiconductors and reaction centra of photosynthetic bacteria have been undertaken.